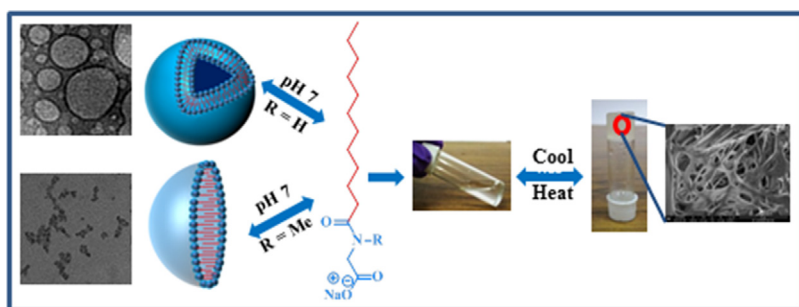# A comparison of the self-assembly behaviour of sodium *N*-lauroyl sarcosinate and sodium *N*-lauroyl glycinate surfactants in aqueous and aqueo-organic media

Deepnath Bajani [a,1], Debmalya Gharai [b,1], Joykrishna Dey [a,*]

[a] *Department of Chemistry, Indian Institute of Technology Kharagpur, Kharagpur 721302, India*
[b] *NMR Research Center, Department of Solid State and Structural Chemistry, Indian Institute of Science, Bangalore 560012, India*

GRAPHICAL ABSTRACT

ARTICLE INFO

ABSTRACT

Self-assembly of surfactants is influenced by various intermolecular interactions and molecular structure, which dictate packing of molecules in the aggregate and its microstructure. Hydrogen-bonding between amide groups plays a key role in the self-assembly process of *N*-acyl amino acid surfactants (NAAS). The self-assembly properties of two NAAS, sodium *N*-lauroyl sarcosinate (SLS) and sodium *N*-lauroyl glycinate (SLG) that differ only in the head-group structure were compared in aqueous and aqueo-organic media by using a number of methods, including surface tension fluorescence, dynamic light scattering, calorimetry, and microscopy. It was observed that aggregate formation is more favoured in SLG. Studies revealed that while SLS formed small spherical micelles, SLG produced unilamellar vesicles in pH 7 buffer above critical micelle concentration at 25 °C. The stability of SLG vesicles with respect to pH and temperature was also investigated. Furthermore, both SLG and SLS were found to gelify aquo-organic mixtures of varying composition upon heat-cool treatment. Their gelation behaviour was compared by measuring minimum gelation concentration, molecular packing, and morphology and mechanical stability of the thermoreversible gels. The difference in self-assembly behaviour in water as well as in aqueo-organic mixtures was attributed to the steric repulsion and hydrogen-bonding interaction at the head-group of the molecules.

© 2018 Elsevier Inc. All rights reserved.

1. Introduction

Surfactants have been well known for centuries for their essential use as detergents, wetting agents, emulsifiers, foaming agents and dispersants [1–5]. However, the interest towards surfactant

chemistry has outgrown extensively in recent years for their applications in foods and pharmaceutics [6–10]. *N*-Acyl-L-amino acids (NAAs) constitute an intriguing class of biocompatible surfactants. They are mild, dermatologically soft, and highly biodegradable, and hence are currently used in detergents, foams and shampoos. The cleavable amide group offers an excellent optimization of chemical stability and biodegradability [11]. The self-assembly properties of NAAs have been studied both in aqueous and organic solvents [12–16]. Miyagishi et al. [17] have investigated aggregation behavior of a series of sodium salts of *N*-dodecanoyl-L-amino acids. These surfactants were found to form micellar structures in aqueous solution. Dey and co-workers have explored the self-assembly behaviour of a series of sodium salts of N-(11-acylamidoundecanoyl)-L-amino acids [18–20] and N-(4-*n*-alkyloxybenzoyl)-L-amino acids [21,22] in water. The intermolecular H-bonding between amide groups and between head groups was shown to be responsible for bilayer formation.

Sarcosine (*N*-methylglycine) is a metabolite of glycine. It is metabolized to glycine by the enzyme sarcosine dehydrogenase, while glycine-*N*-methyl transferase generates sarcosine from glycine [23]. Sarcosine is present in muscles and other body tissues and in foods, such as egg yolks, ham, vegetables, legumes, etc. It has recently been identified as a biomarker for invasive prostate cancer [24,25]. Also, sarcosine supplementation may be used to alleviate depression and schizophrenia and to improve cognition [26]. Thus, a sarcosine derived surfactant, sodium *N*-lauroyl sarcosinate (SLS) has immense biological and industrial significance. It is used in a number of cosmetic formulations and in soaps [27–30].

Gad and coworkers [31] have evaluated interfacial and thermodynamic parameters of SLS in water in the temperature range of 20–65 °C by surface tension and conductivity studies. Moulik et al. [32] have studied interfacial and bulk behaviours of SLS. They have compared the critical micelle concentration (*cmc*) values of SLS measured by various techniques, e.g. surface tension, conductometric and spectroscopic methods. The *cmc* was found to be method dependent. They have also looked into the effects of pH, temperature and salinity on the *cmc* value of SLS. A year later, Bordes and coworkers [33] demonstrated the role of amide bond in the self-assembly of SLS and sodium *N*-lauroyl glycinate (SLG). Besides studying their adsorption behaviour at solid surfaces by quartz crystal microbalance with dissipation (QCM-D) monitoring and by surface plasmon resonance (SPR), they have also evaluated the *cmc* of both the surfactants by tensiometric and conductometric titrations and measured the surface excess and Krafft temperature. Earlier our group has investigated interaction of SLS with micelle-forming cationic surfactants *N*-cetylpyridinium chloride (CPC) and *N*-dodecylpyridinium chloride (DPC) and demonstrated coexistence of disk-like micelles with mean hydrodynamic diameter (d_h) of about 3–10 nm and pH-responsive small unilamellar vesicles ($d_h \sim$ 50–200 nm) at different molar ratios, including 1:1 in dilute (1 mM) catanionic solution [34]. In contrast, catanionic mixtures of SLS with *N*-dodecyltrimethyl-ammonium chloride (DTAC) or *N*-cetyltrimethylammonium chloride (CTAC) formed only spherical micelles ($d_h \sim$ 2–6 nm) at different molar ratios [35]. In a recent paper, Popova and co-researcher have reported the ^{1}H and ^{13}C chemical shifts and ^{1}H spin-relaxation times of SLS in aqueous solution and mixed binary systems in the presence of co-surfactants [36]. More recently, Rudra el al. have studied the binding interaction of SLS with haemoglobin and myoglobin proteins [37].

It appears from the foregoing literature reports that despite its widespread use, detailed comparative study of the self-assemblies formed by SLS and SLG in aqueous solutions still needs attention. In particular, the shape and size of the aggregates formed by these surfactants, and the polarity and viscosity of the microenvironment of the aggregates have not been addressed elsewhere. Also, the self-assembly of these surfactants in organic media has not been reported. The present paper attempts to fill these gaps and presents a thorough investigation on the self-assembly properties of both the surfactants in aqueous as well as in aqueous-organic media. We have extensively studied the self-assembly properties of SLS and SLG in neutral buffered solution by using a number of methods, including surface tension (ST), fluorescence, dynamic light scattering (DLS), isothermal titration calorimetry (ITC), rheology, X-ray diffraction, and optical and electron microscopy. The focus of this work is to investigate the role of hydrogen-bonding (H-bonding) interaction on the self-assembly of these surfactants.

2. Materials and methods

2.1. Materials

Lauroyl chloride (98%), coumarin-153 (C153, 99%), *N*-phenyl-1-naphthylamine (NPN, 98%), and 1,6-diphenyl-1,3,5-hexatriene (DPH, 98%) were purchased from Sigma-Aldrich (India). Fluorescence probes, NPN, DPH and C153 were recrystallized from acetone-ethanol mixture before use. Analytical grade glycine (>99%), sarcosine (>99%), and triethylamine (TEA, >98%) were obtained from Sisco Research Laboratories Pvt. Ltd. (India). Dimethylsulfoxide (DMSO, $\geq$99%), dimethylformamide (DMF, >99.5%), *N*-methyl-2-pyrrolidone (NMP, >99%), and tetrahydrofuran (THF, >99%) were purchased from Merck (India). Honyon International, Inc. (China) supplied ethanol (>99.9%) used in the studies. CDCl$_3$ (Cambridge Isotope Laboratory, USA) and D$_2$O (Sigma-Aldrich, India) were used as NMR solvents. THF and TEA were distilled for synthesis of SLG and SLS. The details of synthetic procedure and spectroscopic data for chemical identification are given under "Electronic Supporting Information" (ESI).

2.2. Methods

2.2.1. General instrumentation

^{1}H- and ^{13}C NMR spectra were recorded on an AVANCE DAX-500 (Bruker, Sweden) 500 MHz NMR spectrometer. A Perkin Elmer (USA) RX1 FTIR spectrometer was used for recording FTIR spectra. Melting point was determined using InstInd (Kolkata, India) melting point apparatus with open capillaries. The pH measurements were done with digital pH meter (Model 111, India) using a glass electrode. Aqueous phosphate buffer (pH 7) was prepared from Milli-Q water (resistivity >18.2 MΩ cm).

2.2.2. Surface tension

Surface tension (ST, γ) measurements were performed on a GBX 3S (France) surface tensiometer equipped with a Julabo F12 (Germany) water-circulating bath using Du Nüoy ring detachment method. The instrument was calibrated and checked by measuring the ST of Milli-Q water (18 MΩ cm) before the experiment. To a 10 mL phosphate buffer (20 mM, pH 7) solution taken in a Teflon beaker, aliquots of surfactant stock solution (prepared using same buffer) were added in measured volume. The solution was gently stirred and γ (mN m^{-1}) was measured after 10 min of equilibration. Each measurement was repeated twice.

2.2.3. Steady-state fluorescence measurements

Fluorescence emission spectra of NPN and C153 probes were recorded on a Hitachi F-7000 (Japan) spectrophotometer. For fluorometric titration, the final concentration of NPN and C153 was 1 μM. The solutions containing NPN and C153 were excited at 340 and 420 nm, respectively.

2.2.4. Fluorescence anisotropy

A Perkin Elmer LS-55 luminescence spectrometer (USA) was used to measure the steady-state fluorescence anisotropy (r) of DPH in the presence of the surfactants. The instrument is equipped with a polarization accessory that uses the L-format instrumental configuration and a thermostated and magnetically stirred cell housing that allowed temperature control. The anisotropy was calculated employing the equation [38]:

$$r = (I_{VV} - GI_{VH})/(I_{VV} + 2GI_{VH}) \qquad (1)$$

where I_{VV} and I_{VH} are the fluorescence intensities polarized parallel and perpendicular to the excitation light, and G ($=I_{VH}/I_{HH}$) is the instrumental grating factor. The software supplied by the manufacturer automatically determined the G-factor and r. For each measurement, the r value was recorded over an integration time of 10 s. For each sample, an average of five readings was accepted as the value of r. A stock solution of 1 mM DPH was prepared in super dry methanol. Aliquots of this stock solution were added to the surfactant solutions so that the final concentration of the probe was ~1 µM. The anisotropy measurements were carried out at different surfactant concentrations in the temperature range 25–75 °C. Before measurement started, each solution was equilibrated for 10 min at the experimental temperature. The sample was excited at 350 nm and the emission intensity was followed at 450 nm using excitation and emission slit width of 2.5 nm and 2.5–10.0 nm, respectively. A 430 nm cut-off filter was placed in the emission beam to eliminate the effect, if any, of scattered radiation.

2.2.5. Time-resolved fluorescence measurements

An Easylife™ X (Optical Building Blocks Corporation, USA) time-resolved instrument was used to measure the fluorescence lifetime of DPH probe. The light source was a 380 nm diode laser. The time-resolved decay curves were analysed by use of single exponential or bi-exponential iterative fitting program. The best fit was judged by the χ^2 value (0.8–1.2) and by the randomness of residual plot.

2.2.6. Determination of microviscosity

The viscosity (inverse of fluidity), η_m, of the microenvironment of the self-assemblies was measured by use of DPH probe. The η_m was calculated from the values of r and rotational correlation time (τ_R) of DPH probe using Debye–Stokes–Einstein relation [39]:

$$\eta_m = kT\tau_R/v_h \qquad (2)$$

where v_h is the hydrodynamic volume (313 Å^3) [40] of the DPH molecule. The τ_R was calculated using Perrin's equation [38]:

$$\tau_R = \tau_f(r_o/r - 1)^{-1} \qquad (3)$$

where r_o (=0.362) [41] and τ_f are the steady-state fluorescence anisotropy of DPH in a highly viscous solvent and measured fluorescence lifetime of DPH in surfactant solution, respectively.

2.2.7. Dynamic light scattering

The hydrodynamic size distribution of the aggregates formed in aqueous solution was measured by dynamic light scattering (DLS) technique. The DLS measurement employed a Zetasizer Nano ZS (Malvern Instrument Lab., UK) equipped with a He-Ne laser working at 4 mW (λ_o = 632.8 nm). Each sample was allowed to equilibrate inside the DLS optical system chamber for 5 min prior to the start of the measurement. All measurements were performed at 25 ± 0.1 °C. The scattering intensity was measured at 173° to the incident beam. The instrument automatically performed several runs in order to produce a monomodal or multimodal size distribution profile.

2.2.8. Zeta potential

To evaluate the surface charge density of the aggregates, zeta potential was measured on a Zetasizer Nano ZS (Malvern Instrument Lab, UK) instrument using folded capillary cell. The reported value is the average of three readings. In principle, the Zetasizer Nano instrument calculates the zeta potential by determining the electrophoretic mobility and then applying the Henry equation. The electrophoretic mobility is obtained by performing an electrophoresis experiment on the sample and measuring the velocity of the particles using laser Doppler velocimetry (LDV) using Henry equation [42]:

$$U_E = \frac{2\varepsilon\zeta f(ka)}{3\eta} \qquad (4)$$

where U_E is electrophoretic mobility, ε is dielectric constant, ζ is Zeta potential, η is viscosity and $f(ka)$ is Henry function. Two values (either 1.5 or 1.0) are generally used as approximations for the $f(ka)$ determination. For small particles in low dielectric constant media, $f(ka)$ is 1.0. This is referred to as the Huckel approximation. Non-aqueous measurements generally use the Huckel approximation. For aqueous samples with moderate electrolyte concentration, the Smoluchowski approximation is used and $f(ka)$ = 1.5.

2.2.9. Microcalorimetry

The isothermal titration calorimetry (ITC) experiments were performed using a Microcal iTC$_{200}$ (Malvern Instruments Ltd., UK) microcalorimeter. In a microsyringe of capacity 40 µL, concentrated stock surfactant solution was taken and injected step by step at equal time spacing of 180 s, into pH 7 buffer kept in the calorimeter cell of capacity 200 µL under constant stirring at 400 rpm. The temperature of the calorimeter was maintained at 25 ± 0.01 °C. The heat absorbed or released at every injection produced a thermogram. Enthalpy changes were calculated using the software provided by the manufacturer. Each run was duplicated to check reproducibility of the results.

2.2.10. Transmission electron microscopy

The morphology of the aggregates was visualized with high resolution transmission electron microscope (JEM–2100 HRTEM, JEOL, Japan) operating at an accelerating voltage of 120 kV. For negative staining, aqueous uranyl acetate (1% w/v) was used. Briefly, in a microcentrifuge tube, 10 mg of uranyl acetate was dissolved in 1 mL of Milli-Q water and was stirred to a light yellow colour solution. The solution was filtered with a 0.22 µm syringe filter. The filtrate wrapped in aluminium foil was stored in the dark for future use. Now, using a fresh syringe (BD Glide with TBL 31G-U40, Becton Dickson India Pvt. Ltd., New Delhi, India), a 2 µL tiny droplet of the sample solution was cast on to a 400 mesh size carbon-coated copper grid, allowed to stand for 2 min, and the grid was blotted from its edge with a piece of Whatman filter paper. A piece of parafilm was cut off and attached to a petri dish by pressing down the periphery of the parafilm. Three droplets (10 µL each) of aqueous uranyl acetate (1% w/v) and four droplets of Milli-Q water (10 µL each) were placed on the parafilm in a row. The grids with the sample were successively touched with the droplets of stain solution and Milli-Q water with forceps. After 1–2 min, the grids were blotted and air-dried overnight on a petri dish. The detail of staining protocol is available elsewhere [43].

2.2.11. Gelation test

Gelation abilities of the surfactants were examined by measuring minimum gelation concentration (MGC). In a screw-capped glass vial, a weighed amount (~10 mg) of solid gelator was dispersed in a solvent by heating in a water bath and then allowed to cool at 25 ± 0.1 °C in a temperature controlled water bath

(Julabo F12, Germany). The material was considered to be a gel when it did not flow upon "inversion of the vial" [44].

2.2.12. Optical microscopy

The optical micrographs (OM) of the gels were taken on a Leica DM LM optical image analyzer microscope (Leica, Germany). A small volume (20 μL) of the hot sols was poured onto a glass slide which was then sealed with a cover slip and placed in the microscope.

2.2.13. Scanning electron microscopy

The morphology of the xerogels was visualized by field emission scanning electron microscopy (FESEM). At first, the hot dispersion (sol) was placed on an aluminium foil, allowed to cool, and air-dried at room temperature. A layer of gold was sputtered on top to make conducting surface, and finally the specimen was transferred onto the Zeiss Supra-40 FESEM (Germany) operating at 5 kV to get the micrographs.

2.2.14. X-ray diffraction measurements

For X-ray diffraction (XRD) measurements, the organogel samples were prepared on a glass slide and air-dried at room temperature. The experiments were carried out on Bruker AXS, Diffractometer D8 (Germany), using Ni-filtered Cu $K_{\alpha 1}$ (154.05 pm) radiation. The operating voltage and current of the instrument were 40 kV and 30 mA, respectively. The spectrum was recorded at room temperature between 2 and 10° in the 2θ scan mode in steps of 0.02° in 2θ at a scan speed of 0.001 s^{-1}.

2.2.15. Rheology

The rheological measurements were performed on Anton Paar rheometer (Model MCR 102) using parallel-plate (PP-25, diameter 25 mm) geometry with a constant tool gap of 100 μm. The rheometer was fitted with a solvent trap and a peltier device that controls temperature within 25 ± 0.1 °C. The preformed gel was gently scooped out from the vial with a spatula and placed on the rheometer plate. An equilibration time of 10 min was allowed before measurement of each sample. The frequency sweep measurements of storage modulus (G′), loss modulus (G″) were performed at a constant stress in the linear viscoelastic region (LVER).

2.2.16. Software and statistical data analysis

All statistical analyses and plotting were performed by OriginPro8 software. NMR spectra were analysed by MestReNova v7.1.0-9185 software (Mestrelab Research S.L). ChemDraw Ultra v12.0.2.1076 software (Cambridgesoft, PerkinElmer Informatics, USA) was used as a drawing tool of chemical structures and reaction schemes. Measurements were done in replicates to check the reproducibility of results. Average values and standard deviation (SD) were calculated and the results were represented as mean ± SD, wherever possible.

3. Results and discussion

3.1. Self-assembly in aqueous media

3.1.1. Surface activity

ST (γ) measurement is a common method for the determination of surface activity and other interfacial properties. The γ values of both SLS and SLG were measured in phosphate buffer (pH 7.0, 20 mM) at 25 °C. The variation of γ (mN m^{-1}) with [surfactant] is shown by the plots in Fig. 1. The γ-value decreases gradually with [surfactant] and reaches a plateau (γ$_{min}$) at the critical aggregation concentration (cmc) (indicated by arrows). This suggests continuous adsorption of surfactant molecules at the air/water interface
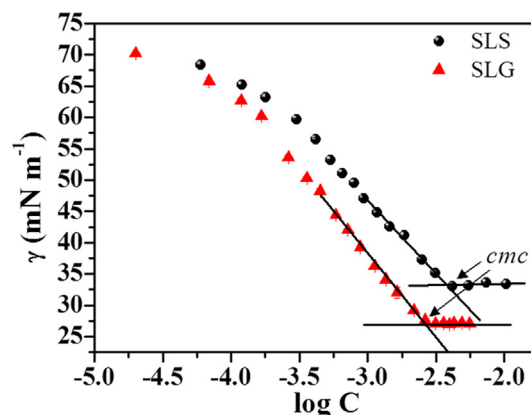

Fig. 1. Variation of γ with logC of SLS and SLG in phosphate buffer (20 mM, pH 7) at 25 ± 1 °C.

followed by surface saturation and self-aggregation. The cmc values thus obtained are listed in Table 1. The cmc values are much less than the corresponding values reported in the literature [33]. This is possibly due to the lower pH (7.0) and higher ionic strength, μ (=0.044 M) of the aqueous solution employed in the present investigation. However, the cmc value of SLS closely matches with the value (3.98) reported by Rudra et al. [37] As discussed later, at pH 7.0, existence of acid form (as a result of hydrolysis) reduces electrostatic repulsion between —COO$^-$ head groups through acid-soap dimer formation thereby facilitating aggregation. It is observed that cmc value of SLG is slightly less than that of SLS, suggesting aggregate formation is more favoured in the case of SLG surfactant, which is consistent with the results reported by Bordes et al. [33] This can be attributed to steric hindrance of the N-methyl group, which prevents acid-soap dimer formation by SLS. Relatively low value of γ$_{min}$ (Table 1) also suggests that SLG is more surface-active than SLS. Further, it is evident from the pC_{20} (pC_{20} is defined as negative logarithm of the bulk-phase concentration necessary to reduce the γ of water by 20 mN m^{-1}) values in Table 1 that SLS is less surface active than SLG.

Determination of cmc by ST method also provides an opportunity to determine the packing of the surfactant molecules at the air/water interface. A substance that lowers the surface energy is present in excess at or near the surface. The maximum surface excess or saturation adsorption (Γ_{max}) was calculated from using Gibbs adsorption equation [45]:

$$\Gamma_{max} = -\frac{1}{2.303nRT}\frac{d\gamma}{d\log C} \tag{5}$$

where C is the concentration of the surfactant, N$_A$ is Avogadro number, R = 8.314 J K^{-1} mol^{-1} is the gas constant, T is the temperature in K, and n = 2 for dilute solutions of 1:1 ionic surfactant [45]. The Γ_{max} value can be used to calculate the minimum surface area per surfactant molecule (A$_{min}$) using Eq. (6) [46]:

$$A_{min} = \frac{1}{\Gamma_{max}N_A} \tag{6}$$

The interfacial parameters (Γ_{max}, and A$_{min}$) thus obtained is tabulated in Table 1. Considering the difference in values of pH and μ, the data are very similar to those reported by Bordes et al. [33] The higher Γ_{max} value of SLG suggests that the surfactant molecules at the interface are more tightly packed compared to SLS. This is reflected by the values of A$_{min}$ which is less in the case of SLG. As discussed above, the steric hindrance rendered by the N-methyl group in SLS results in a less tight packing and hence higher value of A$_{min}$. The low A$_{min}$ value for SLG is indicative of the formation of closed bilayer vesicles in solution [45].

Table 1
The values of *cmc*, pC$_{20}$, γ_{min}, Γ_{max}, and A_{min} of SLS and SLG obtained from ST measurements; data in column Flu were obtained from the fluorescence titration curves in Fig. S8(a).

Surfactant	*cmc* (mM)		γ_{min} (mN m^{-1})	pC$_{20}$	$\Gamma_{max} \times 10^6$ (mol m^{-2})	A_{min} (Å^2 molecule^{-1})
	ST	Flu				
SLS	3.8 ± 0.3	3.9 ± 0.3	33 ± 1	3.19	2.07	80.2
SLG	2.6 ± 0.2	3.1 ± 0.4	27 ± 1	3.45	2.40	69.2

3.1.2. Fluorescence probe studies

The self-assembly of the surfactants was investigated by fluorescence probe method. In order to (i) show self-assembly formation, and (ii) probe the local environment of the aggregates formed by the surfactant molecules, we used NPN, C153, and DPH as extrinsic fluorophores. NPN and C153 can sense the polarity of the microenvironment formed, while DPH is a good viscosity probe. The probe molecules are poorly soluble in water (<1 μM) and are weakly fluorescent in aqueous medium.

In aqueous buffer (pH 7, 20 mM), NPN exhibited a very weak fluorescence with emission maximum (λ_{max}) around 460 nm. In the presence of the surfactant, NPN showed large blue shift (about 32–38 nm) with almost 18 and 24 folds increments in intensity for SLG and SLS, respectively (Fig. S7). This clearly suggests that the surfactant molecules self-assemble to form aggregates with a microenvironment that is much less polar compared to bulk water. The variation of relative fluorescence intensity (F/F$_o$; where F$_o$ and F are the fluorescence intensities in the absence and presence of the surfactant, respectively) and spectral shift ($\Delta\lambda = \lambda_{max}$(buffer) $- \lambda_{max}$(sample)) of NPN with [surfactant] are plotted in Fig. S8. The sigmoid feature of the plots suggests a transition followed by equilibrium between single-tailed surfactant monomers and the aggregates formed, where the concentration corresponding to the initial breakpoint (indicated by arrows in the figure) of the plots give the *cmc* values (Table 1). Thus, within the experimental error limits, the *cmc* values obtained by fluorescence titration are closely similar to the corresponding value obtained by ST method.

3.1.3. Micropolarity

The fluorescent probe, C153 is widely used to measure polarity of the microenvironments of aggregates formed by surfactant molecules [47]. In aqueous buffer (pH 7, 20 mM), the fluorescence emission spectrum ($\lambda_{max} \approx 550$ nm) of C153 probe is weak in the absence of surfactant. With increasing concentration of surfactant, the λ_{max} exhibits a shift to shorter wavelengths along with a gradual increase of fluorescence intensity (Fig. S9). There is a good correlation between the frequency of fluorescence emission of C153 and the micropolarity of the microenvironment of the aggregates. This micropolarity is expressed by π^*-polarity scale, which is defined by the following equation [48]:

$$\bar{v}_{em} = 21.217 - 3.505\pi^* \tag{7}$$

where $\bar{v}_{em}$ [in 10^3 cm^{-1}] is the wavenumber corresponding to the emission maximum of C153. The SLS and SLG exhibited the emission maximum at 539 nm, indicating a 14 nm blue shift. Using λ_{max} = 539 nm, we obtained π^*-value to be 0.76 for both the surfactants which is comparable to the polarity of nitromethane (0.75) or dichloromethane (0.73) [48]. Thus, the presence of amide hydrogen atom in the case of SLG apparently has little or no effect on micropolarity of the self-assemblies formed. This indicates that the probe molecules are solubilized within the micellar core constituted by the hydrocarbon chains.

3.1.4. Microviscosity

Steady state fluorescence anisotropy measurements were carried out with varying surfactant concentrations at 25 °C. Fluorescence anisotropy (*r*) of DPH probe predicts the rigidity of its microenvironment [49,50]. The *r* value for micelles usually falls in the range 0.05–0.10, whereas bilayer aggregates or vesicles usually have *r* > 0.14 [40]. From the experimental *r* values presented in Table S1, it is evident that SLG forms bilayer aggregates in contrast to SLS that forms micelles in pH 7 buffer. Further, at any concentration, SLG has greater *r* value than SLS, suggesting a more rigid microenvironment of the aggregates in the case of SLG. In SLS, however, the presence of the *N*-methyl group might foster a sort of steric crowding, thus restricting the molecules to come in close proximity to form acid-soap dimer (Fig. 2) [51,52]. This means weaker packing of the hydrocarbon chains of SLS monomers, and thus DPH molecule can rotate more freely within its microenvironment. On the other hand, the absence of *N*-methyl group facilitates acid-soap dimer formation in the case of SLG. As a result, the intermolecular amide hydrogen-bonding (H-bonding) is facilitated in SLG thus enhancing self-assembly that produces a more rigid (viscous) bilayer membrane as shown in Fig. 2. In fact, a strong intermolecular interaction among SLG molecules in the solid state is reflected in its solid-liquid melting temperature (68–70 °C) which is higher than that of SLS (45–47 °C).

In order to determine the microviscosity (η_m) of the aggregates formed by the surfactants, the fluorescence decay of DPH was measured. Fluorescence lifetime (τ_f) of DPH is known to depend on the environment. Usually, τ_f of DPH in nonpolar non-viscous solvent is observed to be 4.0 ns [53] It is noteworthy that the time-resolved intensity profile of DPH fits well (χ^2 = 0.80–1.2) to single exponential decay for both the surfactants. The experimental τ_f values of DPH between 5.0 and 6.0 ns clearly indicate the formation of viscous hydrophobic region by these surfactants. Using the experimental *r* and τ_f data (Table S1) of DPH, the η_m value of the aggregates was evaluated. The η_m value for SLS (21 mPa s) in pH 7 is comparable to the micelle forming SDS (η_m = 16 mPa s)[40] surfactant. However, the higher η_m value for SLG (59 mPa s) could be arising from more rigid microstructure, like vesicles.

3.1.5. Thermodynamics of self-assembly formation

ITC was performed to evaluate the thermodynamic parameters and hence the driving force for the self-assembly process. The standard Gibbs free energy ($\Delta_{mic}G°$) of micellization was calculated using the following equation [54,55]:

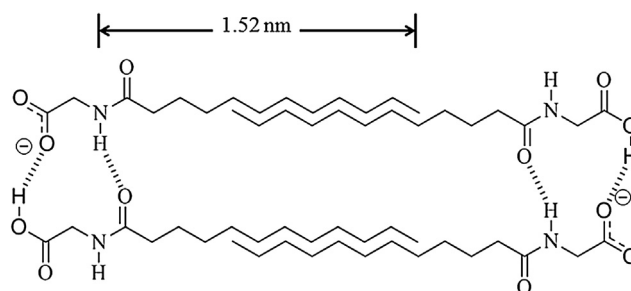$$\Delta_{mic}G° = (1 + \beta)RT \ln X_{cmc} \tag{8}$$

Fig. 2. Schematic diagram of the bilayer structure formed by SLG molecules in aqueous buffer.

Table 2
Thermodynamic parameters ($\Delta_{mic}H^o$, $\Delta_{mic}G^o$, $T\Delta_{mic}S^o$) of micellization, and *cmc* values of SLS and SLG at 25 ± 1 °C.

Surfactant	*cmc* (mM)		$\Delta_{mic}H^o$ kJ mol^{-1}	$\Delta_{mic}G^o$ kJ mol^{-1}	$T\Delta_{mic}S^o$ kJ mol^{-1}
	ST	Flu			
SLS	3.8 ± 0.3	3.9 ± 0.3	26.91 ± 0.52	−13.66 ± 0.06	40.57 ± 0.52
SLG	2.6 ± 0.2	3.1 ± 0.4	36.88 ± 0.19	−15.01 ± 0.39	52.09 ± 0.43

where β is the degree of counterion binding. As the measurement was done in phosphate buffer (20 mM, pH 7) the β-value is expected to be higher and therefore it was taken to be equal to 0.8 for the anionic surfactants. This is consistent with the low *cmc* value compared to that in pure water. In fact, the β-value is usually taken as 0.8 for anionic surfactant and 0.0 for zwitterionic surfactants [56]. X_{cmc} is the *cmc* expressed in mole fraction units, and R and T have their usual meaning. The standard state was hypothetical state of zero concentration. The standard entropy change ($\Delta_{mic}S^o$) for the micellization was calculated from the equation [56]:

$$\Delta_{mic}S^o = (\Delta_{mic}H^o - \Delta_{mic}G^o)/T \qquad (9)$$

where $\Delta_{mic}H^o$ stands for the standard enthalpy of micellization. The average value of *cmc* by two methods (tensiometry and fluorimetry) was taken to calculate $\Delta_{mic}G^o$. $\Delta_{mic}H^o$ value was obtained by subtracting the enthalpy of non-micellar region and that of micellar region [54]. The thermograms are presented in Fig. S10 of ESI and the data are collected in Table 2. For both SLS and SLG, the self-assembly process is observed to be endothermic as reflected by the positive $\Delta_{mic}H^o$ values. Similar value of $\Delta_{mic}H^o$ was also reported by researchers [32]. A large negative $\Delta_{mic}G^o$ value guarantees spontaneity of the self-assembly processes for both the surfactants. As $|T\Delta_{mic}S^o| > |\Delta_{mic}H^o|$, the self-assembly process is entropy-driven. It is well known that micellization is a typical consequence of hydrophobic effect with disruption of "structured water" and increase in entropy [57,58]. The larger negative $\Delta_{mic}G^o$

and higher $\Delta_{mic}S^o$ value in the case of SLG suggests that self-aggregation is more favoured in comparison to that in SLS. As both surfactants have the same hydrocarbon chain length this could be due to the difference in head-group interactions during self-assembly formation. This is indicated by the difference in $\Delta_{mic}H^o$ values of the surfactants which is associated with the amide H-bonding (Fig. 2) in the case of SLG.

3.1.6. Hydrodynamic size and shape

The size distribution histograms at two different concentrations of SLS (in Fig. 3(a, b)) support formation small micelles of $d_h \sim 3$ nm. However, unlike SLS, SLG formed large aggregates of $d_h \sim 57$ nm (Fig. 3(a, b)) indicating existence of vesicles in dispersion. Thus the ST, fluorescence, and DLS results are consistent with each other.

The shape of the aggregates was visualized with HRTEM. The negatively stained HRTEM micrographs of SLS and SLG dispersions in pH 7 are shown in Fig. 3(c, d). The images clearly reveal the formation of micelles by SLS (Fig. 3c) and of vesicles by SLG surfactant (Fig. 3d). The vesicles formed by SLG have hydrodynamic diameter in the range 20–90 nm and is consistent with the results of DLS measurements. The vesicles appear to be unilamellar at the measured surfactant concentration. In contrast, the SLS micelles have diameter of about 3–10 nm. Thus, three independent measurements, fluorescence anisotropy, HRTEM, and DLS are in good agreement with each other.
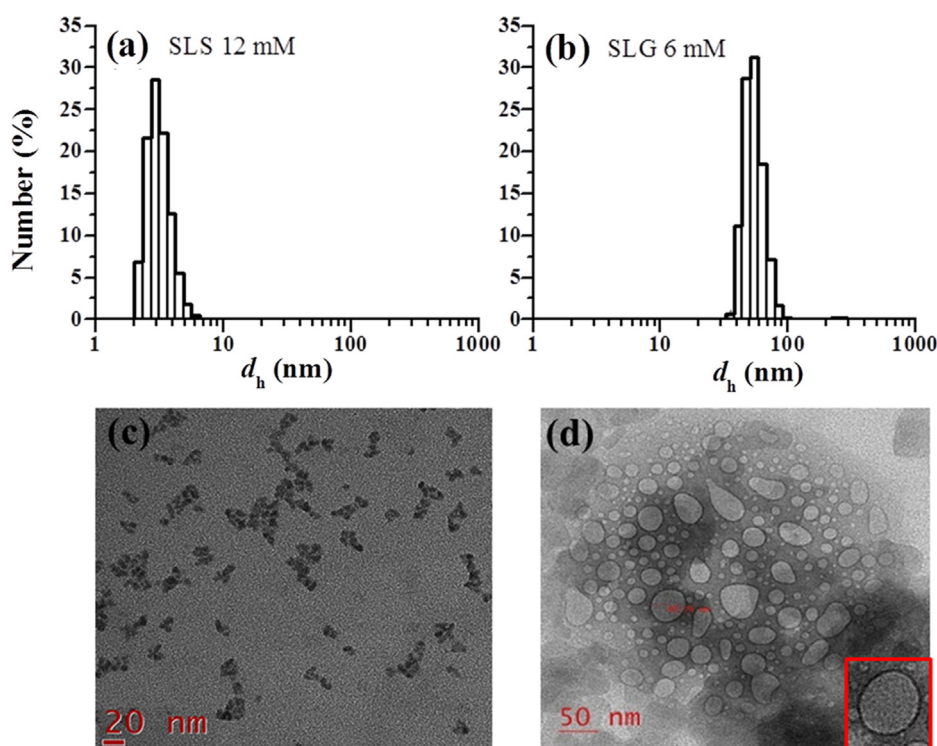

Fig. 3. Size distribution histogram of (a) SLS (12 mM) and (b) SLG (6 mM) dispersion in pH 7 phosphate buffer at 25 °C; Negatively stained (with 1% w/v uranyl acetate) HRTEM images of micelles (c) of SLS (12 mM) and vesicles (d) of SLG (6 mM) in pH 7 phosphate buffer.

3.1.7. Aggregate stability

The above experimental studies demonstrate that SLS spontaneously produced micelles and SLG produced unilamellar vesicles (ULVs) in pH 7 buffer at 25 °C. It is well known that spontaneous surfactant self-assemblies always remain in a kinetic as well as thermodynamic equilibrium with the monomers and their physical stability can be altered by external stimuli like temperature, pH, etc. Therefore, to study the stability of the self-assemblies formed by the surfactants, we performed DLS and zeta-potential measurements at different pHs, and fluorescence anisotropy at different temperatures.

Colloidal dispersions are subject to instability in several forms. The dispersed particles can stick to each other (aggregation, coagulation, and flocculation), they can stick to surrounding surfaces (deposition), or they can phase-separate under gravity (sedimentation or creaming). These mechanisms all can be counteracted by strong electrostatic repulsion. Zeta potential is a measure of the surface charge density of the particles and determines degree of repulsion between adjacent, similarly charged particles. The high ζ-potential value of SLS (-26 mV) and SLG (-63 mV) presented in Table S1 indicates reasonable stability of the aggregates in dispersion. It should also be noted that the ULVs of SLG have a greater magnitude of ζ-potential than the micelles formed by SLS and therefore are expected to be more stable.

Temperature is an important stimulus that can affect molecular self-assemblies. Since increase in temperature causes an increase of the degree of counter-ion ionization and head-group repulsions as well as disruption of "structured water", the driving force for aggregation is diminished [59]. In bilayer membranes, increased temperature increases membrane fluidity and the extent of water penetration into the bilayer [60,61]. The thermal stability of the aggregates was investigated by recording fluorescence anisotropy (r) of the DPH probe in the temperature range of 25–70 °C. It is clear from Fig. 4a that the r value initially decreases with increase in temperature and then attains a constant value, for both SLS and SLG. However, the lowering of anisotropy is more prominent in SLS than in SLG. In the case of SLG, the r-value lies in the vesicular range (>0.14) [40] even at 70 °C. The initial lowering of r value can be attributed to the weakening of hydrophobic interactions among the hydrocarbon chains in micelle core or in bilayers due to thermal agitation. Besides anisotropy, we also performed DLS measurements with the surfactant dispersions at 25 and 37 °C. The size distribution histograms in Fig. 5(a, b) and (d, e) show that upon increasing the temperature from 25 to 37 °C, there is no significant change in mean d_h value of SLS micelles (12 mM, pH 7) or SLG vesicles (6 mM, pH 7) thus showing reasonably good thermal stability of the ULVs at the physiological temperature.

The stability of aggregates with variation of pH was also studied by monitoring fluorescence anisotropy of DPH probe. The data

presented in Fig. 4(b) show that for SLG, the r value decreases with the increase of pH following a sigmoid curve. The pK_a value obtained from the inflection point of the curve is ca. 7.3 which is consistent to the pK_a value of corresponding fatty acid (8.0) [52]. This means that below pH 7.3 the SLG molecules exist mostly in the acid ($-COOH$) form. In fact, this is why the SLG is less soluble in water at room temperature. The relatively higher aqueous solubility of SLS is due to the *N*-methyl group that weakens interactions between surfactant molecules which is easily overcome by surfactant-water H-bonding interactions.

Further, the size distribution histograms in Fig. 5(a, c) show that the mean d_h of SLS micelles and SLG vesicles remained almost unaltered on increasing the pH from 7 to 10. However, on decreasing the pH from 7 to 5.5 both SLS (12 mM) and SLG (6 mM) dispersion on standing showed appearance of shiny crystals (Fig. 5f). A plausible explanation for the decrease of r-value of DPH is that at alkaline pH, the surfactant molecules remain mainly in the salt form ($-COO^-$) which increases electrostatic repulsions among the surfactant head groups thereby making the packing of hydrocarbon chains less tight in the vesicle bilayer. On the other hand, in acidic pH, the carboxylate anion gets protonated, causing precipitation of the acid form of the surfactant. Thus the ULVs of SLG are unstable in acidic pH.

3.2. Self-assembly in aquo-organic media

3.2.1. Gelation behaviour

Low-molecular-mass organogelators (LMOGs) have received considerable interest over the past decades [62–64]. LMOGs self-assemble frequently into 3D fibrillar networks as a consequence of a variety of non-covalent interactions, such as London dispersion forces, van der Waals forces, hydrogen bonding, and electrostatic and interfacial attractions or repulsions. It was accidentally found that both SLG and SLS form weak or partial hydrogel in water at very high ($>50\%$, w/w) concentrations. Because gelation depends on moderate solubility of the surfactant in the solvent, the solubility could be lowered by mixing organic solvents to water. Indeed, both SLG and SLS were found to gel DMSO/water, DMF/water and NMP/water solvent mixtures. Table 3 presents the MGC values of the two gelators at 25 °C in different aquo-organic mixtures. It is evident from the data in Table 2 that in each of the solvent mixtures tested SLG gel has a lower MGC value than SLS gel. One plausible explanation could be that the presence of methyl group on the amide nitrogen atom in SLS sterically hinders the gelator molecules to come close to each other, thereby affecting their self-aggregation. However, in the case of SLG, the absence of *N*-methyl group and the presence of amide H atom facilitate 3D network structure, via intermolecular H-bonding (see Fig. 3) which imparts better stability to the gels formed. It is also observed that
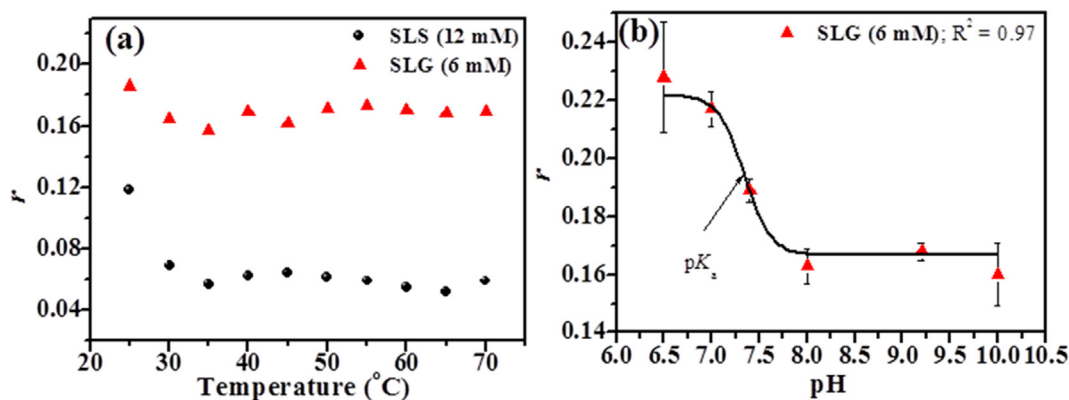

Fig. 4. Variation fluorescence anisotropy (r) of DPH (a) with temperature in SLS (12 mM) and SLG (6 mM) in pH 7.0 buffer, and (b) with pH in SLG (6 mM).
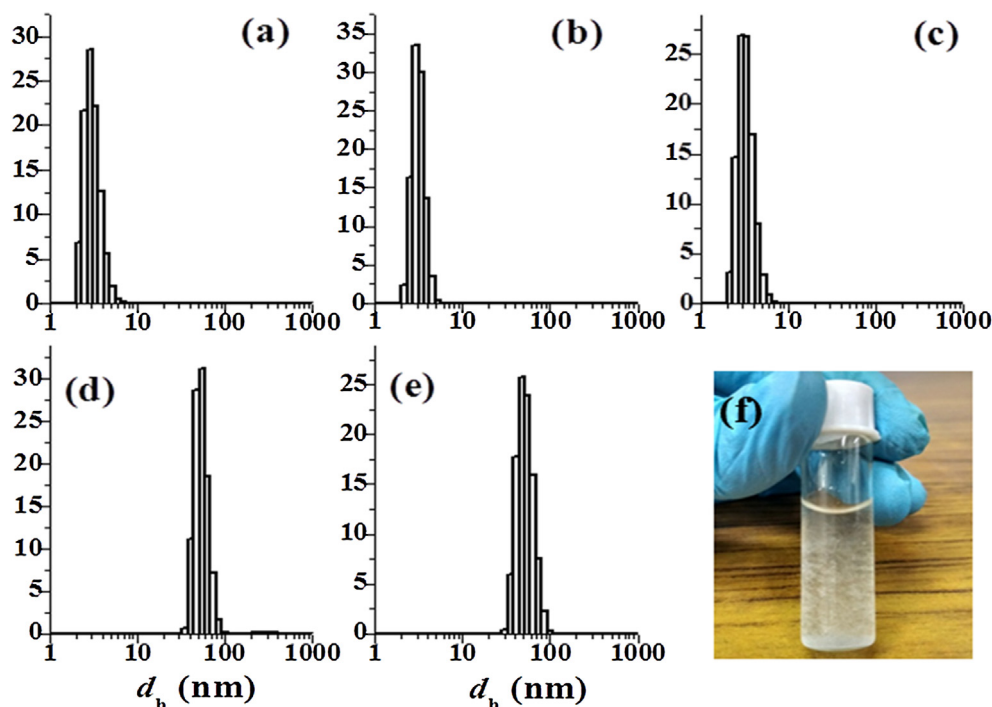
Fig. 5. Size distribution histograms of (a) SLS (12 mM, pH 7, 25 °C), (b) SLS (12 mM, pH 7, 37 °C), (c) SLS (12 mM, pH 5.5, 25 °C), (d) SLG (6 mM, pH 7, 25 °C), and (e) SLG (6 mM, pH 7, 37 °C); (f) photograph showing crystallization of SLG (6 mM) in pH 5.5 at room temperature.

Table 3
MGC values (in % w/v) of the gels in different aquo-organic mixtures of varying composition at 25 ± 0.1 °C: PG = partial gel, WG = weak gel, P = precipitation.

Solvent system	Solvent:water (v/v)	MGC (±0.1% w/v)	
		SLG	SLS
NMP/water	9:1	4.16	8.03
	8:2	3.18	9.60
	7:3	3.39	13.86
	6:4	4.45	15.70
	5:5	7.58	PG
	4:6	13.21	PG
DMF/water	9:1	3.59	9.75
	8:2	3.08	8.59 (WG)
	7:3	4.18	14.13 (WG)
	6:4	4.8	PG
	5:5	8.67	P
	4:6	18.95	P
DMSO/water	9:1	2.28	7.07
	8:2	2.43	5.27
	7:3	2.85	5.62
	6:4	2.20	9.24
	5:5	2.61	11.78
	4:6	4.41	22.53 (PG)
	3:7	9.96	P

in each mixed solvent system, the MGC value is minimum at a certain vol% of water. Above or below this vol% of water, the MGC value increases, which means gelation is favoured only at a specific polarity of the medium.

3.2.2. Morphology of gels

The gel structure was established by measuring rheology of the gels. The storage modulus (G') and loss modulus (G'') were measured as a function of angular frequency (ω) (Fig. 6). The plots show that in the low frequency range, both G′ and G″ are almost independent of frequency, confirming gel structure. Also, at any given frequency G′ is much higher than G″, indicating the elastic nature of the gels.

The morphology of the organogels was studied by optical microscopy (OM). Fig. 7 shows the optical micrographs of the organogels formed by SLS and SLG in different solvents. The OM images clearly exhibit fibrillar aggregates of high aspect ratio, forming 3-D network structures. The FESEM micrographs of the xerogels shown in Fig. 8 suggest that SLG forms high aspect ratio flakes, needles or entangled ribbons (Fig. 8(a–c)), while SLS mostly forms long ribbons (Fig. 8(d–f)) in different aquo-organic mixtures. The difference in gel morphology of the two gelators can the attributed to the tendency of SLG molecules to form highly ordered aggregates like crystals due to strong intermolecular H-bonding interactions in comparison to SLS.

3.2.3. X-ray diffraction studies

In support of the structures shown by the FESEM images of the organogels, we have performed XRD measurements using respective air-dried gel films. The XRD technique is particularly useful to decipher the intermolecular packing pattern and dimensions of the aggregate structures. The XRD spectra of the organogels of SLS and SLG in different solvent mixtures are presented in Fig. S11. The periodicity of the reflection peaks (at a ratio of 1:2:3) in the XRD spectra clearly indicates the presence of layered or ordered lamellar structures. The values of inter-layer spacing (d) obtained for SLS and SLG gels are 2.52 nm and 2.51 nm, respectively. This is slightly less than twice the hydrocarbon chain length (1.52 nm) of the surfactants, suggesting interdigitation (see Fig. 2) of the hydrocarbon tails of the surfactants in the bilayer aggregates.

3.2.4. Driving force for gelation

It is well-known that a balanced participation of hydrophilicity and hydrophobicity is important for self-aggregation of amphiphilic molecules. However, in strongly H-bonding and polar solvents, hydrophobic forces provide a major contribution towards the overall stabilization of the assemblies. Thus, the major driving force for gelation by SLS and SLG appears to be van der Waals interactions
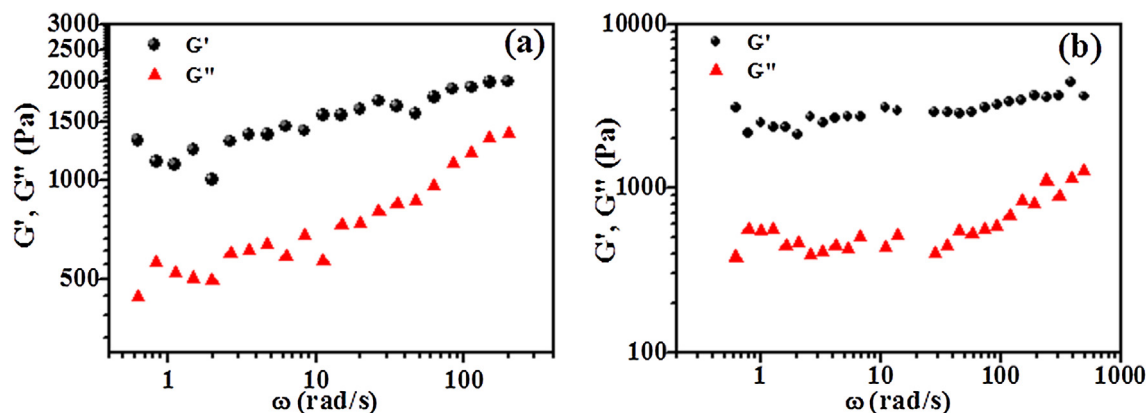
Fig. 6. Variations of G′ and G″ with frequency (ω) of the aquo-organogels of (a) SLS and (b) SLG in NMP-water (8:2 v/v) at 25 °C.
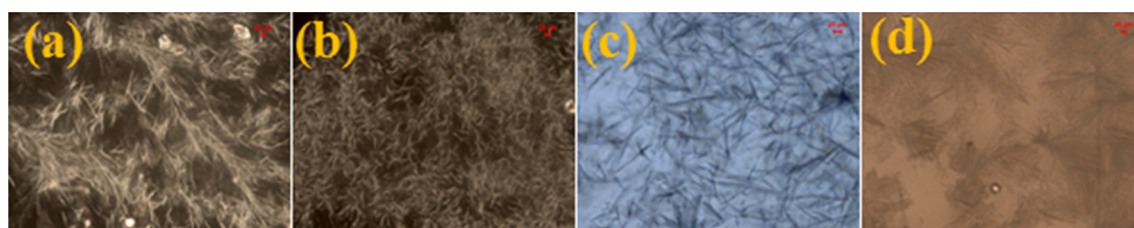

Fig. 7. Representative optical micrographs of gels of: (a) SLS in NMP/water (8:2), (b) SLG in DMF/water (8:2), (c) SLG in DMSO/water (8:2), and (d) SLG in NMP/water (8:2).
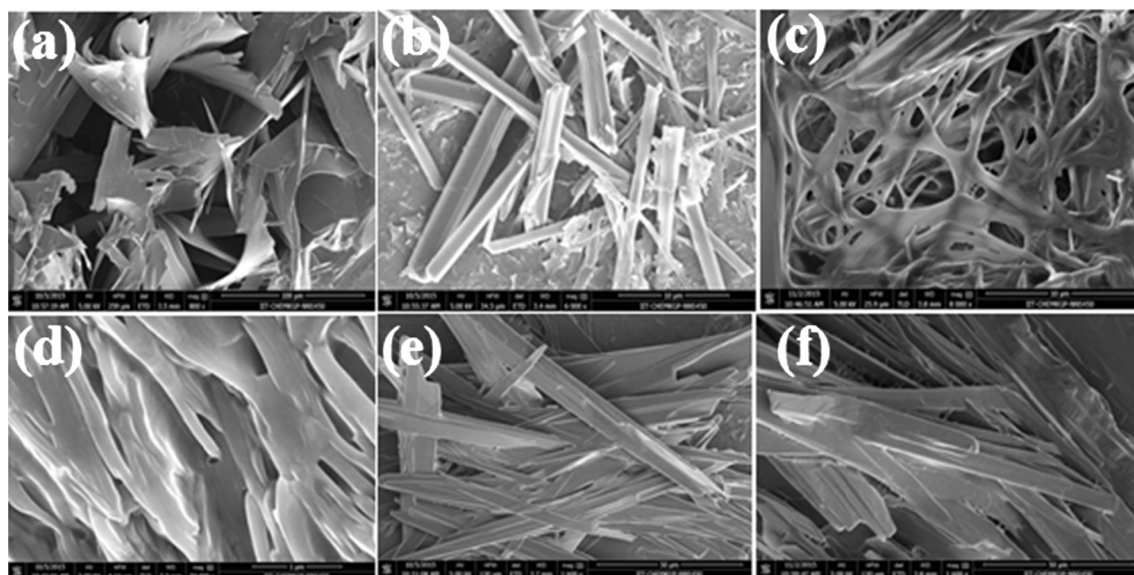

Fig. 8. Representative FESEM micrographs of xerogels of: (a) SLG in DMF/water (8:2), (b) SLG in DMSO/water (8:2), (c) SLG in NMP/water (8:2) (below MGC), (d) SLS in DMF/water (8:2), (e) SLS in DMSO/water (8:2), and (f) SLS in NMP/water (8:2).

between hydrocarbon chains. However, since the hydrocarbon chain lengths are equal for both gelators, the difference in gelation abilities is due to the difference in interactions between head groups. Thus SLG has lower MGC values than SLS in all the solvent mixtures studied. This indicates that SLG self-aggregates more tightly than SLS in which the *N*-methyl group imparts steric hindrance. Consequently, as discussed above the acid-soap dimer formation as well as amide H-bonding is prohibited in the case of SLS. On the other hand, the absence of *N*-methyl group in SLG affords a better packing of molecules and hence one-dimensional growth of aggregates producing fibres is facilitated.

As gels behave like solids, the role of H-bonding interaction in the self-assembly/gelation process may further be understood by comparing the FTIR spectra of SLS and SLG in the solid state (Figs. S1 and S2) as well as in xerogels (Fig. S12). In the solid state, the amide C=O stretch appeared at 1628 cm^{-1} for SLS and at 1619 cm^{-1} for SLG. This red shift of amide C=O stretch in the case of SLG clearly suggests involvement of strong H-bonding in the solid state. Further, the solid state asymmetric C=O stretch of carboxylate shows intense peak at 1603 cm^{-1} for SLS and at 1597 cm^{-1} for SLG. Thus, the carboxylate C=O stretch also shifted to lower wavenumber in SLG relative to SLS, indicating the presence of

stronger H-bonding interaction. However, there was no notable difference in the symmetric C=O stretching frequency of carboxylate (1408 cm^{-1} for SLS and 1407 cm^{-1} for SLG). To further envision the role of H-bonding in the self-assembly, we measured the FTIR spectra of the xerogels of both SLS and SLG (Fig. S12). Similar results were observed as was found in the solid state. In the xerogel of SLG in DMSO/water (7:3), the amide C=O shifted to 1620 cm^{-1} while it appeared at 1629 cm^{-1} in the case of SLS xerogel. Also, the asymmetric carboxylate C=O for SLS and SLG xerogels appeared at 1603 and 1596 cm^{-1}, respectively. These results also support the participation of H-bonding interaction in the gel state.

4. Conclusions

In summary, the self-assembly properties of two amino acid based surfactants, SLS and SLG were studied thoroughly both in aqueous buffers and aquo-organic media of varying compositions. As also reported in the literature, SLG is less soluble in water at neutral pH at room temperature, which is due to the strong H-bonding interaction between amide groups [33]. Indeed, for the same reason, the solid-liquid melting point of SLG is greater than that of SLS surfactant. The difference in the values of stretching frequencies of the C=O bond in SLG and SLS also support H-bonding interaction at the head group. The pK_a of SLG at room temperature being equal to 7.3, the acid-soap dimer formation is more favoured at pH 7.3. But the acid-soap dimer formation in SLS is sterically hindered by the *N*-methyl group, which can be either in trans or cis conformation [65]. This is also reflected in the slightly lower *cmc* value of SLG compared to that of SLS. Thus despite having equal hydrocarbon tail lengths, the aggregate formation is more favoured in the case of SLG. The *cmc* value of both SLS and SLG surfactants in phosphate buffer (pH 7), however, is much less than the value in water at pH 8.5 [33]. Also because of the steric hindrance due to the *N*-methyl group and absence amide H-bonding, SLS is less surface-active than SLG, as indicated by the pC_{20} values. Although their structures differ only in the *N*-methyl group at the surfactant head, SLS produced small spherical micelles, but SLG produced small unilamellar vesicles (SUVs) in aqueous buffered solution (pH 7) above *cmc* at 25 °C. The stronger H-bonding interaction in the case of SLG favoured formation of acid-soap dimer which leads to the formation of bilayer aggregates. Thus the present study demonstrates that head-group structure has a strong influence on the surface adsorption as well as on the aggregate morphology. Since solubilisation capacity of vesicles is greater than that of small micelles, it can be concluded that SLG can act as a better cleansing agent than SLS. Further it has been shown that because of stronger amide H-bonding, the SUVs are stable even at 70 °C. Since the packing of hydrocarbon chains in the bilayer membrane of SUVs becomes less tight at alkaline pH, they can have potential applications as pH-responsive drug delivery vehicle. The present study also demonstrates that both the surfactants form thermoreversible opaque gels in aquo-organic media, but with a moderately high MGC values (2–15% w/v). In each mixed solvent system, the MGC value is minimum at a certain vol% of water which means gelation is favoured only at a specific polarity of the medium. Studies reveal that SLG gels are formed at lower MGC values compared to SLS irrespective of the solvents. Strong H-bonding interaction leads to the generation of crystalline aggregates of low aspect ratio in the case SLG gels, but relatively weaker H-bonding interaction in SLS results in the formation of elongated aggregates of high aspect ratio, thus favouring more entangled 3-D network gel. Thus SLG can find applications in the formulation of various cosmetic products. In consistence with the literature reports, the present study led to the conclusion that strong H-bonding interaction favours crystallization of the surfactants, but relatively weaker H-bonding interaction leads to gelation [66,67].

5. Conflict of interest

The authors declare no competing financial interests.

Appendix A. Supplementary material

Supplementary data associated with this article can be found, in the online version, at https://doi.org/10.1016/j.jcis.2018.06.026.

References

[1] M.R. Porter, Handbook of Surfactants, second ed., Blackie Academic & Professional, London, 1994.
[2] K. Holmberg, B. Kronberg, B. Lindman, Surfactants and Polymers in Aqueous Solution, second ed., John Wiley & Sons Ltd, England, 2003.
[3] T.F. Tadros, Applied Surfactants: Principles and Applications, Wiley-VCH, Germany, 2005.
[4] U. Zoller (Ed.), Handbook of Detergents, Part E: Applications, Surfactants Science Series, vol. 141, CRC Press, Taylor & Francis Group, New York, 2009.
[5] L.L. Schramm, E.N. Stasiuk, D.G. Marangoni, Surfactants and their applications, Annu. Rep. Prog. Chem., Sect. C 99 (2003) 3–48.
[6] B.J. Boyd, D.V. Whittaker, S.-M. Khoo, G. Davey, Lyotropic liquid crystalline phases formed from glycerate surfactants as sustained release drug delivery systems, Int. J. Pharm. 309 (2006) 218–226.
[7] C. Sinico, A.M. Fadda, Vesicular carriers for dermal drug delivery, Expert Opin. Colloid Interface Sci. 7 (2002) 276–281.
[8] C.J. Drummond, C. Fong, Surfactant self-assembly objects as novel drug delivery vehicles, Curr. Opin. Colloid Interface Sci. 4 (2000) 449–456.
[9] R. Srinivas, S. Samanta, A. Chaudhuri, Cationic amphiphiles: promising carriers of genetic materials in gene therapy, Chem. Soc. Rev. 38 (2009) 3326–3338.
[10] S.D. Palma, B. Maletto, P. Lo Nostro, R.H. Manzo, M.C. Pistoresi-Palencia, D.A. Allemandi, Potential use of ascorbic acid-based surfactants as skin penetration enhancers, Drug Dev. Ind. Pharm. 32 (2006) 821–827.
[11] M. Stjerndahl, K. Holmberg, Synthesis, stability, and biodegradability studies of a surface-active amide, J. Surfactants Deterg. 8 (2005) 331–336.
[12] M. Shinitzky, R. Haimovitz, Chiral surfaces in micelles of enantiomeric N-palmitoyl and N-stearoylserine, J. Am. Chem. Soc. 115 (1993) 12545–12549.
[13] J. Song, Q. Cheng, S. Kopta, R.C. Stevens, Modulating artificial membrane morphology: pH-induced chromatic transition and nanostructural transformation of a bolaamphiphilic conjugated polymer from blue helical ribbons to red nanofibers, J. Am. Chem. Soc. 123 (2001) 3205–3213.
[14] X. Du, V. Hlady, Monolayer formation on silicon and mica surfaces rearranged from N-hexadecanoyl-L-alanine supramolecular structures, J. Phys. Chem. B 106 (2002) 7295–7299.
[15] C. Boettcher, B. Schade, J.H. Fuhrhop, Comparative cryo-electron microscopy of noncovalent N-dodecanoyl-(D-and L-) serine assemblies in vitreous toluene and water, Langmuir 17 (2001) 873–877.
[16] H. Kawasaki, M. Souda, S. Tanaka, N. Nemoto, G. Karlsson, M. Almgren, H. Maeda, Reversible vesicle formation by changing pH, J. Phys. Chem. B 106 (2002) 1524–1527.
[17] S. Miyagishi, T. Asakawa, M. Nishida, Hydrophobicity and surface activities of sodium salts of N-dodecanoyl amino acids, J. Colloid Interface Sci. 131 (1989) 68–73.
[18] S. Roy, J. Dey, Effect of hydrogen-bonding interactions on the self-assembly formation of sodium N-(11-acrylamidoundecanoyl)-L-serinate, L-asparaginate, and L-glutaminate in aqueous solution, J. Colloid Interface Sci. 307 (2007) 229–234.
[19] S. Roy, J. Dey, Spontaneously formed vesicles of sodium N-(11 acrylamidoundecanoyl)-glycinate and L-alaninate in water, Langmuir 21 (2005) 10362–10369.
[20] S. Roy, J. Dey, Self-organization properties and microstructures of sodium N-(11-acrylamidoundecanoyl)-L-valinate and-L-threoninate in water, Bull. Chem. Soc. Jpn. 79 (2006) 59–66.
[21] A. Mohanty, J. Dey, Effect of the headgroup structure on the aggregation behavior and stability of self-assemblies of sodium N-[4-(n-dodecyloxy) benzoyl]-L-aminoacidates in water, Langmuir 23 (2007) 1033–1040.
[22] A. Mohanty, T. Patra, J. Dey, Salt-induced vesicle to micelle transition in aqueous solution of sodium N-(4-n-octyloxybenzoyl)-L-valinate, J. Phys. Chem. B 111 (2007) 7155–7159.

[23] https://pubchem.ncbi.nlm.nih.gov/compound/sarcosine#section=Top. (PubChem is an open chemistry database maintained by the National Center for Biotechnology Information (NCBI), a component of the U.S. National Library of Medicine, which is part of the United States National Institutes of Health (NIH). Accessed on 27th Feb 2018.

[24] A. Sreekumar, L.M. Poisson, T.M. Rajendiran, A.P. Khan, Q. Cao, J.D. Yu, et al., Metabolomic profiles delineate potential role for sarcosine in prostate cancer progression, Nature 457 (2009) 910–914.

[25] Z. Heger, M.A. Merlos Rodrigo, P. Michalek, H. Polanska, M. Masarik, V. Vit, M. Plevova, D. Pacik, T. Eckschlager, M. Stiborova, V. Adam, Sarcosine up-regulates expression of genes involved in cell cycle progression of metastatic models of prostate cancer, PLoS One 11 (2016) 1–20.

[26] C.Y. Lin, S.Y. Liang, Y.C. Chang, S.Y. Ting, C.L. Kao, Y.H. Wu, G.E. Tsai, H.Y. Lane, Adjunctive sarcosine plus benzoate improved cognitive function in chronic schizophrenia patients with constant clinical symptoms: a randomised, double-blind, Placebo-Controlled Trial, World J. Biol. Psychiatry 18 (2017) 357–368.

[27] R.S. Lanigan, Final Report on the Safety Assessment of Cocoyl Sarcosine, Lauroyl Sarcosine, Myristoyl Sarcosine, Oleoyl Sarcosine, Stearoyl Sarcosine, Sodium Cocoyl Sarcosinate, Sodium Lauroyl Sarcosinate, Sodium Myristoyl Sarcosinate, Ammonium Cocoyl Sarcosinate and Ammonium Lauroyl Sarcosinate, Int. J. Toxicol. 20 (Suppl. 1) (2001) 1–14. Published by Informa Healthcare.

[28] E.J. Castillo, W.W. Han, S.H. Gerson, Use of Certain Anionic Amino Acid Based Surfactants to Enhance Antimicrobial Effectiveness of Topically Administrable Pharmaceutical Compositions. US Patent 6,146,622, 2000.

[29] T.V. Orr, A.D. Sabatelli, Skin Conditioning Composition and Method. European Patent EP0283165, 1992.

[30] Colgate Dental Cream with Gardol advertisement in Life Magazine, May 29, 1963 page 4. (via Wikipedia: <https://en.wikipedia.org/wiki/Sodium_lauroyl_sarcosinate>).

[31] E.A.M. Gad, M.M.A. El-Sukkary, D.A. Ismail, Surface and thermodynamic parameters of sodium N-acyl sarcosinate surfactant solutions, J. Am. Oil Chem. Soc. 74 (1997) 43–47.

[32] G.B. Ray, S. Ghosh, S.P. Moulik, Physicochemical studies on the interfacial and bulk behaviors of sodium N-dodecanoyl sarcosinate (SDDS), J. Surfact. Deterg. 12 (2009) 131–143.

[33] R. Bordes, J. Tropsch, K. Holmberg, Role of an amide bond for self-assembly of surfactants, Langmuir 26 (2010) 3077–3083.

[34] S. Ghosh, J. Dey, Interaction of sodium N-lauroyl sarcosinate with N-alkylpyridinium chloride surfactants: spontaneous formation of pH-responsive, stable vesicles in aqueous mixtures, J. Colloid Interface Sci. 358 (2011) 208–216.

[35] Ghosh, Sampad, Interaction of Cationic and Anionic Surfactants: Preparation of pH-Responsive Stable Vesicles for Drug Delivery Applications, Indian Institute of Technology Kharagpur, 2011. (A Ph.D. thesis submitted to Indian Institute of Technology Kharagpur. Accessed via <http://www.idr.iitkgp.ac.in/xmlui/handle/123456789/1097>)

[36] M.V. Popova, D. Michel, Behavior of sodium Lauroyl Sarcosinate in solution and binary mixtures by means NMR, Appl. Magn. Reson. 45 (2014) 353–364.

[37] S. Rudra, S. Dasmandal, A. Mahapatra, Binding interaction of sodium-N-dodecanoyl sarcosinate with haemoglobin and myoglobin: physicochemical and spectroscopic studies with molecular docking analysis, J. Colloid Interface Sci. 496 (2017) 267–277.

[38] J.R. Lakowicz, Principles of Fluorescence Spectroscopy, Plenum Press, New York, 1983.

[39] P. Debye, Polar Molecules, Dover, New York, 1929.

[40] S. Roy, A. Mohanty, J. Dey, Microviscosity of bilayer membranes of some N-acylamino acid surfactants determined by fluorescence probe method, Chem. Phys. Lett. 414 (2005) 23–27.

[41] M. Shinitzky, Y. Barenholz, Dynamics of the hydrocarbon layer in liposomes of lecithin and sphingomyelin containing dicetylphosphate, J. Biol. Chem. 249 (1974) 2652–2657.

[42] D.C. Henry, The cataphoresis of suspended particles. Part I. The equation of cataphoresis, Proc. R. Soc. A 133 (1931) 106–129.

[43] EM Sample Preparation – Contrasting. Copyright © by Leica Mikrosysteme GmbH, Vienna, Austria, Sep 2013. (Available online at <https://www.leica-microsystems.com/fileadmin/academy/2013/Contrasting_final.pdf>)

[44] R.G. Weiss, P. Terech, Molecular Gels: Materials with Self-Assembled Fibrillar Networks, Springer International Publishing AG, Basel, 2006.

[45] M.J. Rosen, Surfactants and Interfacial Phenomena, third ed., Wiley-Interscience, New York, 2004, pp. 60–64.

[46] J.N. Israelachvili, D.J. Mitchell, B.W. Ninham, Theory of self-assembly of hydrocarbon amphiphiles into micelles and bilayers, J. Chem. Soc., Faraday Trans. II 72 (1976) 1525–1568.

[47] D. Bajani, J. Dey, Y. Rajesh, S. Bandyopadhyay, M. Mandal, Spontaneous vesicle formation by γ-aminobutyric acid derived steroidal surfactant: curcumin loading, cytotoxicity and cellular uptake studies, J. Colloid Interface Sci. 507 (2017) 1–10.

[48] M.L. Horng, J.A. Gardecki, A. Papazyan, M. Maroncelli, Subpicosecond measurements of polar solvation dynamics: coumarin 153 revisited, J. Phys. Chem. 99 (1995) 17311–17337.

[49] G. Weber, M. Shinitzky, A.C. Dianoux, C. Gitler, Microviscosity and order in the hydrocarbon region of micelles and membranes determined with fluorescent probes. I. Synthetic Micelles, Biochemistry 10 (1971) 2106–2113.

[50] M. Shinitzky, I. Yuli, Lipid fluidity at the submacroscopic level: determination by fluorescence polarization, Chem. Phys. Lipids 30 (1982) 261–282.

[51] K.P. Ananthapadmanabhan, P. Somasundaran, Acid-soap formation in aqueous oleate solutions, J. Colloid Interface Sci. 122 (1988) 104–109.

[52] J.R. Kanicky, D.O. Shah, Effect of premicellar aggregation on the pKa of fatty acid soap solutions, Langmuir 19 (2003) 2034–2038.

[53] E.D. Cehelnik, R.B. Cundall, J.R. Lockwood, T.F. Palmer, Solvent and temperature effects on the fluorescence of all-trans-1,6-diphenyl-1,3,5-hexatriene, J. Phys. Chem. 79 (1975) 1369–1376.

[54] S. Paula, W. Stis, J. Tuchtenhagen, A. Blume, Thermodynamics of micelle formation as a function of temperature: a high sensitivity titration calorimetry study, J. Phys. Chem. 99 (1995) 11742–11751.

[55] Y. Moroi, Micelle: Theoretical and Applied Aspects, Plenum, New York, 1992.

[56] P.R. Majhi, S.P. Moulik, Energetics of micellization: reassessment by a high-sensitivity titration microcalorimeter, Langmuir 14 (1998) 3986–3990.

[57] B. Kronberg, The hydrophobic effect, Curr. Opin. Colloid Interface Sci. 22 (2016) 14–22.

[58] N.T. Southall, K.A. Dill, A.D.J. Haymet, A view of the hydrophobic effect, J. Phys. Chem. B 106 (2002) 521–533.

[59] S.S. Shah, E. Rehman, Effect of temperature and aprotic solvents on the CMC of sodium dodecyl sulfate, in: H. Kleeberg (Ed.), Interactions of Water in Ionic and Nonionic Hydrates, Springer, Berlin, 1987, pp. 251–255.

[60] T. Patra, S. Ghosh, J. Dey, Spontaneous formation of pH-sensitive, stable vesicles in aqueous solution of N-[4-n-octyloxybenzoyl]-L-histidine, Soft Matter 6 (2010) 3669–3679.

[61] W.V. Kraske, D.B. Mountcastle, Effects of cholesterol and temperature on the permeability of dimyristoylphosphatidylcholine bilayers near the chain melting phase transition, BBA-Biomembranes 1514 (2001) 159–164.

[62] R.G. Weiss, The past, present, and future of molecular gels. What is the status of the field, and where is it going?, J Am. Chem. Soc. 136 (2014) 7519–7530.

[63] N.M. Sangeetha, U. Maitra, Supramolecular gels: functions and uses, Chem. Soc. Rev. 34 (2005) 821–836.

[64] E.R. Draper, D.J. Adams, Low-molecular-weight gels: the state of the art, Chemistry 3 (2017) 390–410.

[65] E. Oshimura, Y. Yamashita, K. Sakamoto, Conformational behavior of N-acylamino acid oil and N-acylamino acid surfactant in aqueous solution, J. Oleo Sci. 56 (2007) 115–121.

[66] A. Pal, R. Das Mahapatra, J. Dey, Comparison of the gelation behaviour of N-substituted tetradecanamide amphiphiles in organic liquids: effect of hydrogen-bonding ability of the head-group, RSC Adv. 4 (2014) 7760–7765.

[67] A. Pal, J. Dey, Organogelation by 4-(N-tetradecanoyl)aminohydroxybutyric acids: effect of hydrogen-bonding group in the amphiphile head, J. Phys. Chem. B 118 (2014) 12112–12120.